An In-Situ Collaborative Robot for Manufacturing in Confined Spaces

Andrew L. Orekhov, Garrison L. H. Johnston, Colette Abah

Vanderbilt University
Department of Mechanical Engineering
Nashville, TN, USA

Contact address:
Andrew Orekhov
Olin Hall Room 101
2400 Highland Ave
Nashville, TN 37212

Contact email:
andrew.orekhov@vanderbilt.edu

Category:
Graduate

Faculty sponsor:
Professor Nabil Simaan
Department of Mechanical Engineering
Vanderbilt University

Acknowledgements:
The participants would like to thank the following people for their support on the project: our faculty advisor Prof. Nabil Simaan, our faculty collaborator on this project Prof. Howie Choset (Carnegie Mellon University), undergraduate students Jin Suh, Lauren Howard, and Cole Sorkness, staff engineer Yizhu Gu, and Vanderbilt machinist John Fellenstein. We also wish to acknowledge funding support from the NSF Award #1734461 and #1445197.

An In-Situ Collaborative Robot for Manufacturing in Confined Spaces

1 Background and Design Overview

1.1.0 Background and Motivation

In some industrial scenarios, workers must enter into confined spaces to perform tasks like assembly, maintenance, and inspection. Examples include maintenance/assembly of aircraft and inspection/cleaning of tanks. Operating in confined spaces is dangerous for workers due to potential environmental hazards and a lack of access for evacuation in an emergency. Furthermore, confined spaces require workers to operate in unergonomoic postures, which increases their physiological burden and risk for musculoskeletal disorders.

Figure 1: Examples of workers operating in confined spaces, which require unergonomic postures and present environmental hazards for workers.

A collaborative robot could alleviate these burdens by supporting the loads needed to carry out the task through cooperative control or by allowing the worker to teleoperate the robot and therefore remove the need for the worker to enter the confined space at all. However, existing robots are challenging to deploy for this application because the robot needs 1) sufficient load carrying capacity and dexterity to reach deep into a confined space, and 2) whole-body situational awareness for navigating the confined space and ensuring safety for the worker.

1.2.0 Design Overview

We present a robot manipulator design that seeks to address these unique challenges of collaborative manufacturing in confined spaces. The robot, which we call an *in-situ collaborative robot* (ISCR), is shown in Fig. 2a. It has 11 degrees-of-freedom (DoF), an overall length of approximately 1.8 meters and a continuous payload carrying capacity of 1.8 kg at the end-effector in its fully cantilevered configuration. Three features of our ISCR design work synergistically to address the requirements of manufacturing in confined spaces. These are 1) statically balanced revolute joints, 2) passively compliant continuum segments with modular actuation, and 3) whole-body proximity and contact sensing along the continuum segments.

The revolute joints, together with a static balancing mechanism that offsets gravitational loads, provide larger load-carrying capacity, particularly at the base of the robot where torque

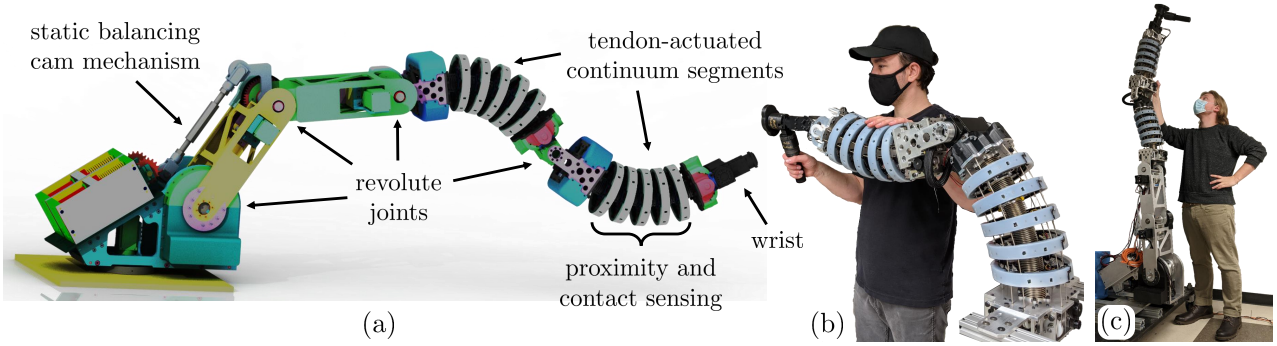

Figure 2: (a) An overview of our proposed in-situ collaborative robot that seeks to address the unique challenges of manufacturing in confined spaces, b) an example of how a worker would physically interact with the robot for cooperative manufacturing, and c) a worker standing next to the full continuum robot assembly.

requirements are high. The continuum segments provide snake-like kinematics that allows the robot to reach deep into a confined space and maneuver within it, and they have integrated mechanical actuation components to provide modular assembly and make the robot easier to reconfigure for new tasks. The passive compliance of the continuum segments provides an additional measure of safety for the worker and makes the robot more forgiving of geometric uncertainty in the environment. The proximity sensing along the body of the continuum segments allows the robot to map the confined space to improve its situational awareness, and the contact sensing provides a means for the robot to detect contact with the environment as well as brace against the environment to further reduce its torque requirements. The proximity and contact sensing, together with pair of load cells mounted on the wrist of the robot, also allow the robot to sense interaction from the worker for cooperative manufacturing, as shown in Fig. 2b.

We believe the unique features of our proposed ISCR will help alleviate the burdens associated with manufacturing in confined spaces by offloading the payload from the user when performing repetitive tasks. In the sections below, we will provide additional detail on these design features and the procedures used to develop the design, including statics/fatigue analysis and multiple stages of physical prototyping.

2 Statically Balanced Revolute Joints

Robots designed for collaborative confined space applications must be simultaneously strong enough to offset the ergonomic load from the user, but also safe enough to pose minimal risk to the operator. In the mechanical design of this robot, we attempt to address this design trade-off in two ways. First, by designing the robot with a mixture of continuum segments and revolute joints, we find a balance between the strength and precision of revolute joints and the passive compliance and dexterity of continuum segments. Second, we incorporate *static balancing* mechanisms into the second and third joints (i.e. the joints subject to the highest gravitational load) that use springs to offset the gravitational load on the joint. This increases the passive safety of the robot by enabling the selection of lower powered actuators than an unbalanced joint with the same overall torque capacity [1]. The decreased joint power minimizes the risk of injuring the robot's operator.

2.1.0 Revolute joint design

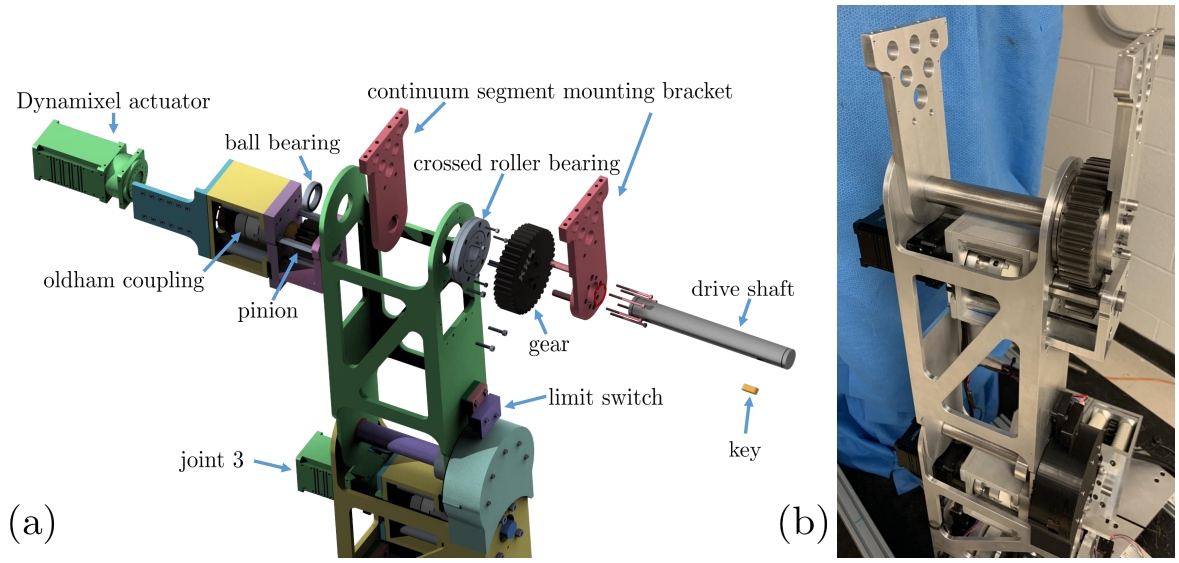

Figure 3: The design of the fourth revolute joint (shown without the continuum segment attached): (a) exploded view rendering (b) photograph of the physical system.

2.1.1 Actuator selection

The robot has a total of seven revolute joints: four at the robot's base, one between the two continuum segments, and two in the robot's wrist. The design of the fourth revolute joint is shown as an example in Fig. 3. Each revolute joint is actuated using a Robotis™ Dynamixel P-Series actuator. The four base actuators and the actuator between the continuum segments are constructed from Robotis PH54-200-S500-R actuators. The part numbers for the wrist are given in the caption of Fig. 4. These actuators were selected because their integrated motor controllers simplified the hardware integration and because of their high power relative to similar actuators. These actuators also provide position, velocity, and current feedback via the Robotis software development kit and have daisy-chained RS485 communication for simplified wiring.

2.1.2 Gear selection

For joints two, three, and four, we added gearing to the output of the Dynamixel actuator to satisfy higher torque requirements for these joints. Each gear pair utilizes 2.5 module, AISI 1045 carbon steel, KHK™ SSG series gears. The selected gear ratios and other performance characteristics of the joints are summarized in Table 1. Note the torque specifications in Table 1 are given excluding the torque reductions provided by the static balancing mechanism. Using the "AGMA Refined Approach" as given in [2], the static safety factor against tooth bending and expected surface and tooth bending fatigue life of the gears was analyzed . The pinion attached to joint 4 is the expected first point of failure for the gears. The pinion has a static safety factor of 1.925 against tooth bending, estimated surface fatigue life of $9.73 * 10^7$ loading cycles, and estimated tooth bending fatigue life of $2.793 * 10^8$ loading cycles, all of which are the lowest amongst all the selected gears.

Table 1: Revolute Joint Performance Specifications

Joint Number	Gear ratio	Max Continuous torque [Nm]	Max. continuous velocity [RPM]
1	1.0	44.7	29
2	4.167	186.25	6.96
3	2.5	111.75	11.6
4	2.5	111.75	11.6
7	1.0	44.7	29
10	1.0	5.1	29.2
11	1.0	1.7	26

2.1.3 Drive shaft selection

The drive shafts used in the revolute joints are constructed from AISI 1045 medium carbon steel. The shaft diameters were selected using the ASME power transmission shaft design equations given in [2]. Using this method, the shafts were designed with a desired static safety factor of 3 and for infinite fatigue life. These calculations where performed using estimated mean and alternating torsional and bending moments.

2.2.0 Wrist with Two DoF and Dual Load Cells

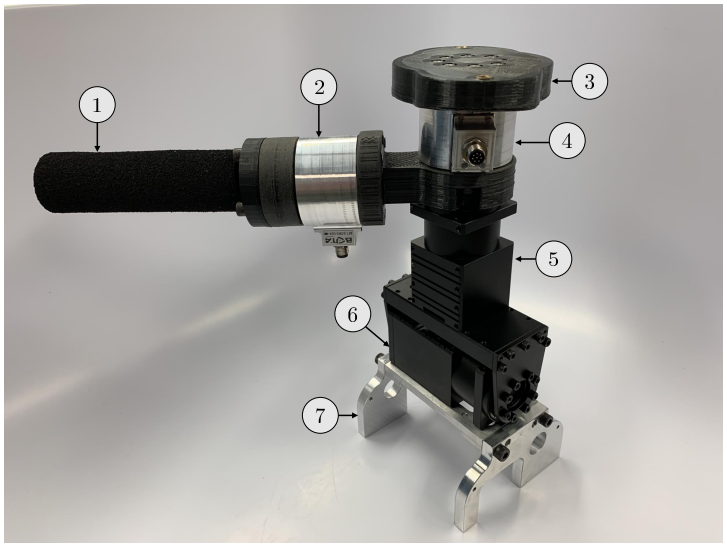

Figure 4: The wrist design: ① user interaction handle, ② Bota Systems™ Rokubi 6-axis force/-torque sensor used to measure user input forces, ③ flange for attaching tools, ④ Rokubi sensor used to measure interaction forces with the environment, ⑤ Dynamixel roll actuator, ⑥ Dynamixel pitch actuator, ⑦ bracket that attaches to the distal continuum segment.

The robot's wrist is constructed from two lower powered Dynamixel P-series actuators (PM42-010-S260-R and PH42-020-S300-R) as shown in Fig. 4. The actuators are arranged to make a pitch-roll wrist configuration, which we selected for its dexterity benefits after simulating the robot in our custom-built MATLAB kinematics simulator. The wrist also includes two Bota Systems™ Rokubi 6-axis force/torque sensors. The first sensor (labeled ② in Fig. 4) measures

the force the user imparts on the robot for admittance control scenarios. The second sensor measures the robot's interaction force with the environment.

2.3.0 Static Balancing Mechanism

As mentioned earlier, in order to offset the gravitational load on the revolute joints subject to the highest gravitational load, we integrated static balancing mechanisms into the second and third revolute joints. The mechanism we used was inspired by [3]. In this method, the designer takes a given translational spring with force-displacement function $f(u)$, attaches a wire to one end of the spring, wraps the wire around an idler pulley, then wraps the wire around a cam. Finally, the wire is terminated at one end of the cam. When the cam rotates, the translational spring extends, causing a moment about the cam's center of rotation. Using the methods given in [3], the cam's profile can be specially designed to generate a desired torque as a function of the cam's angular position $g(\alpha)$. Other works have used counter-balancing masses for static balancing, but this approach, in contrast to the wire-wrapped cam method we pursued, would significantly increase the overall mass and inertia of the robot and therefore reduce worker safety.

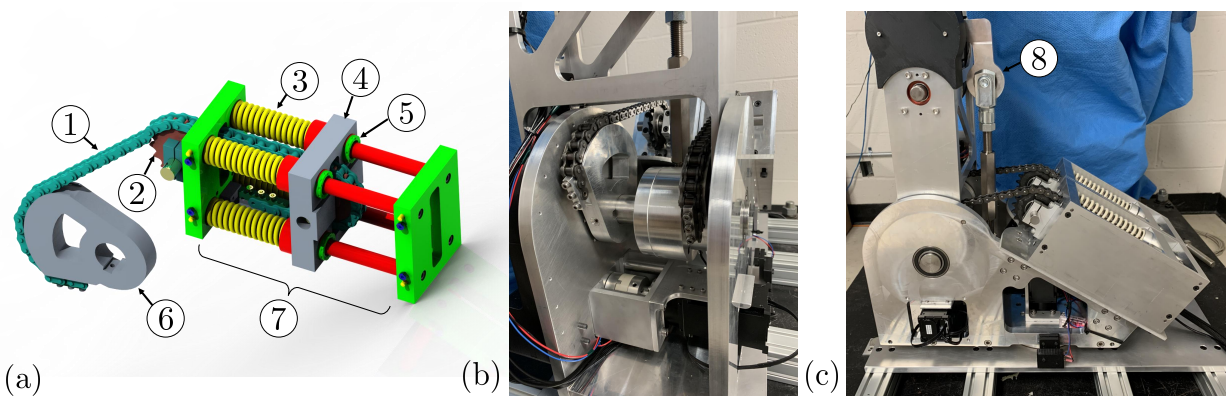

Figure 5: Static balancing mechanism design. (a) A CAD rendering of the design concept: ① roller chain, ② idler sprocket, ③ compression springs, ④ moving platform, ⑤ linear bearings, ⑥ cam, ⑦ 2:1 pulley reduction. (b) Close-up photo of the cams. (c) Side view of the static-balancing design: ⑧ parallelogram mechanism.

The torque generated by each cam depends only on the angle of the joint to which it is attached. However, because the torque on each joint depends on the position of all the subsequent joints, the cams can only approximately balance the gravitational torque in most configurations. For this reason, we used a statics model of the robot with estimated component masses to search the robot's workspace to find the average torque at representative points in the joint's range. We then selected a $g(\alpha)$ function for each cam that approximately passes through the average torques calculated from the workspace search.

Using these desired cam torque functions, cam profiles were calculated using 144 lbf/in translational springs (Lee Spring™ LHL-1250AB-11). However, when analyzing our design, we noticed the cams required an unrealistically large spring stroke. To remedy this, we passed the wire (in our case a roller chain for strength) through a 2:1 pulley reduction to cut the required stroke of the spring in half. This pulley reduction causes the spring constant as felt by the cam to be 1/4 the constant of the spring. Therefore, we designed the system with four 144 lbf/in springs

in parallel (see Fig. 5(a)) in order for the cam design to behave as predicted without requiring unrealistically large spring strokes. The cam for the second revolute joint is rigidly attached to the drive shaft using a key and setscrew. The cam for the third revolute joint is mounted on a bearing on the same shaft. The torque from the cam is then transferred to the third revolute joint using a parallelogram mechanism.

3 Modular Continuum Segments

The ISCR has two tendon-actuated continuum segments that provide snake-like kinematics for the distal portions of the robot to enable it to maneuver deeper into a confined space. The passive compliance of these segments also provides improved safety and robustness to geometric uncertainty in the environment. Unique features of these segments, which we describe in more detail below, include the integrated tendon actuation unit for improved modularity, a torsionally stiff continuum structure for reduced torsional deflections actuated with a 2:1 tendon reduction, and integrated string encoders for sensing deflections of the continuum structure.

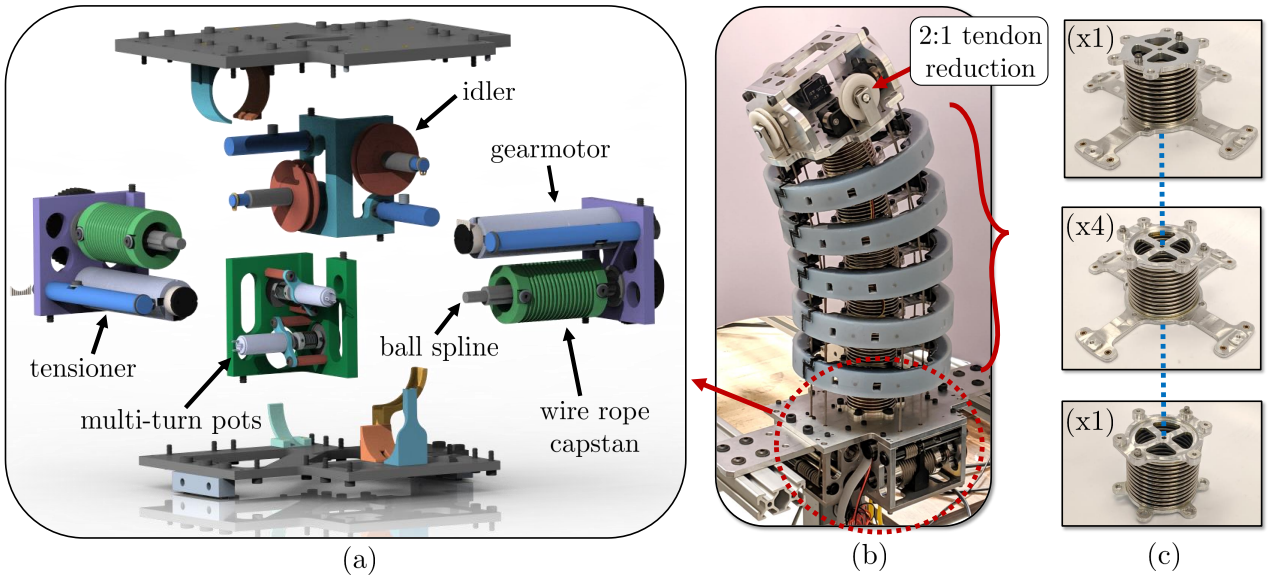

Figure 6: a) Modular actuation unit. b) Full continuum segment assembly. c) Tendon-actuated continuum structure with torsionally stiff metal bellows.

3.1.0 Modular Tendon Actuation Unit

Each continuum segment has 2 actuation DoF. The mechanical components for these two DoF are fully integrated into the base of each segment, as shown in Fig. 6b. These components, shown in the exploded view in Fig. 6a, include a gearmotor with a planetary gearhead (maxon™ DCX/GPX22), a spur gear reduction that drives a wire rope capstan, a ball spline on which the capstan slides to account for wire rope travel, and idler pulleys for guiding the wire-rope from the actuation unit to the continuum structure. Each DoF also has a tensioning shaft that allows the wire rope tension to be set with a torque wrench. There are also two 10-turn potentiometers that allow the robot's home position to be set when initially powered on, which is necessary because

the incremental motor encoders do not provide absolute positioning in a power reset. The motors are controlled at a 2kHz rate using a custom-built motor control box with a PC/104 stack running Real-Time Linux (PREEMPT-RT). Communication between the higher-level Robot Operating System (ROS) controllers and the motor control box is done via UDP at approximately 500 Hz.

The required wire rope force to actuate the structure was determined in simulation using a kinematics/statics model of the robot. Our selected wire rope is a ⌀1.98 mm, 7x49 construction with a breaking strength of 1875 N. We also selected the required gearmotor, spur gear, spline, and ball bearing sizes, based on this statics simulation for given safety factors and fatigue requirements. A unique feature of our wire rope actuation is the use of a idler pulley in the distal endplate of the robot that provides a 2:1 reduction in the tendon force. This force reduction allows us to use a smaller wire rope and reduce the diameters of the drive components.

3.2.0 Continuum Structure

The continuum structure consists of lightweight (33 g), off-the-shelf metal bellows whose torsional stiffness (63 Nm/°) is approximately 1950 times higher than the bending stiffness. This allows the robot to bend in the desired actuation directions and comply to external loads/geometric uncertainty, but prevents the robot from experiencing large deflections in torsion, thereby increasing the load carrying capacity of the segments. As shown in Fig. 6c, these metal bellows are assembled to aluminum intermediate disks using Loctite 326 adhesive to create bellow subassemblies that are then bolted together. Based on the adhesive specifications, the continuum structure can support torsional loads of up to 75 Nm, assuming a safety factor of 3. A 4 mm superelastic nickel-titanium rod is passed through the center of the bellow assemblies to support compression loads, since the metal bellows cannot support significant compression loads. Each of the intermediate disks also contains oil-impregnated bronze bushings through which the actuation tendons pass to reduce the friction between the rope and the intermediate disks.

3.3.0 String Encoders for Shape Sensing

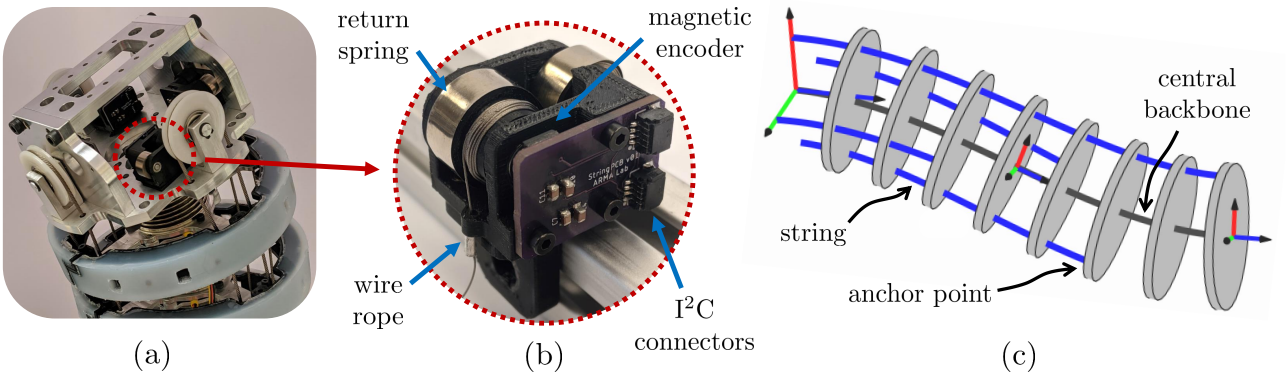

Figure 7: Each continuum segment contains four custom-built string encoders in the distal endplate that provide information about the shape of the robot.

The passive compliance of the continuum segments makes the robot more forgiving of geometric uncertainty and can potentially provide additional passive safety to the robot. However, this compliance presents a challenge in that external forces produce shape changes in the continuum

structure, which introduces uncertainty in the robot's kinematic model. To alleviate this, each continuum segment has four *string encoders* that are used to sense the shape of the segment, as shown in Fig. 7a.

The string encoders in the segment, shown in Fig. 7b, consist of a 0.33 mm diameter wire rope wrapped around a capstan, a constant-torque spring that allows the wire rope to extend/contract, and a magnetic encoder that measures the angle of the capstan. Based on the measured angle of the capstan, we calculate the extension/contraction length of the wire rope. The capstan angle is provided to the higher-level control software via an I^2C interface. The strings are routed within the continuum structure and anchored at different locations within the robot, as shown in Fig. 7c. Based on the measured string lengths, we can update the kinematic model of the robot. We do not delineate the details of the kinematic model here, but refer the reader to [4, 5] for examples of kinematic models that can be used together with string encoders.

4 Multi-modal Sensing Disk Units

Human-robot collaboration in confined spaces presents a unique robot situational awareness challenge. For increased safety, the co-located robot must be able to map its environment, sense neighboring objects, detect and localize contact along its length, and adapt its motion accordingly. To address this challenge, we designed a novel multi-modal sensing disk unit (SDU) that integrates 8 time-of-flight (ToF) sensors, 8 Hall effect sensors, and 8 embedded magnets, distributed around its circumference to enable a) proximity sensing, b) mapping, c) localized contact detection, and d) localized force sensing. The ISCR is endowed with 10 SDU for whole-body sensing and augmented situational awareness.

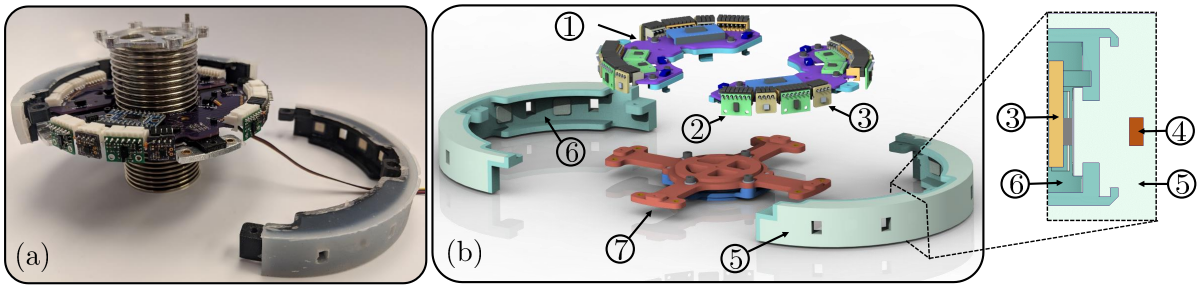

Figure 8: (a) Multi-modal sensing disk unit mounted on a bellow subassembly with the outer cover removed. (b) Exploded view of the SDU components: ① two custom PCBs for multiplexed I^2C communication, ② 8 time-of-flight sensors, ③ 8 Hall effect sensors, ④ magnets used for Hall effect-based contact sensing, ⑤ silicone outer sleeve, and ⑥ a plastic cover over which the silicone is molded. These components are mounted onto ⑦, an intermediate aluminum disk.

Fig. 8(a) and (b) show the design and prototype of a single SDU. Fig. 8(c) shows the details of the components integrated within an SDU. Two custom PCBs ① serve as breakout boards for I^2C communication between the sensors and a Teensy 4.1 microcontroller. Each PCB includes 3 QWIIC I^2C connectors that enable communication with neighboring PCBs (both within the same SDU and crossing to the next SDU). Board edge connectors are used to mount the individual sensors directly to the PCB. This structure facilitates the assembly and troubleshooting of individual sensors, and significantly reduces the number of cables needed. Each PCB is mounted

to a 3D-printed frame, which connects to the core disk via 4 sliding fit joints and a single bolt.

Each SDU contains 8 VL6180X (Pololu) ToF sensors that endow the SDU with proximity sensing and mapping capabilities. We selected ToF sensors with a range of $0 - 100$ mm to accurately measure proximity to a human or an object in the environment, but note that longer range sensors are available as drop-in replacements from the same manufacturer.

The second type of sensor integrated in the SDU is a Hall effect sensor (Melexis MLX90393) that measures the change in magnetic field strength in three orthogonal directions. This feature can be used to detect contact and, when appropriately calibrated, also measure forces. The working principle for contact sensing with these sensors was first explored in [6] and is illustrated in the inlay of Fig. 8(b). For each contact sensor, there is a radially offset magnet embedded in a silicone sleeve. Any external contact with the sensor disk causes the displacement of the magnet within the silicone, which in turn causes a change in magnetic field strength that is measured by the Hall effect sensor. The uncalibrated measurements can be used together with a threshold for "on/off" contact detection. Using offline calibration with a commercial force sensor, this Hall effect setup could also potentially be used as an 3-axis force sensor. We are still validating this force sensing approach, but our preliminary explorations in this direction are promising.

In addition to housing the magnets for Hall effect sensing, the silicone sleeve protects the disk unit from harsh interactions with the environment and the human user. This sleeve was fabricated by casting liquid silicone rubber (Dragon Skin FX Pro) into a custom mold. With a Shore 2A hardness, this elastomer is both flexible enough to detect the motion of the embedded magnet and robust enough to withstand rolling contact with the environment.

4.1.0 Design Iterations and Prototypes

Our procedure for generating the SDU unit design described above involved a series of physical prototypes. Fig. 9 shows three of these design iterations. The design in Fig. 9(a) consisted of a flexible linear potentiometer wrapped around a disk, and protected by a silicone layer. One of the key limitation of this design was that it did not allow for multiple contact points to be detected and differentiated simultaneously.

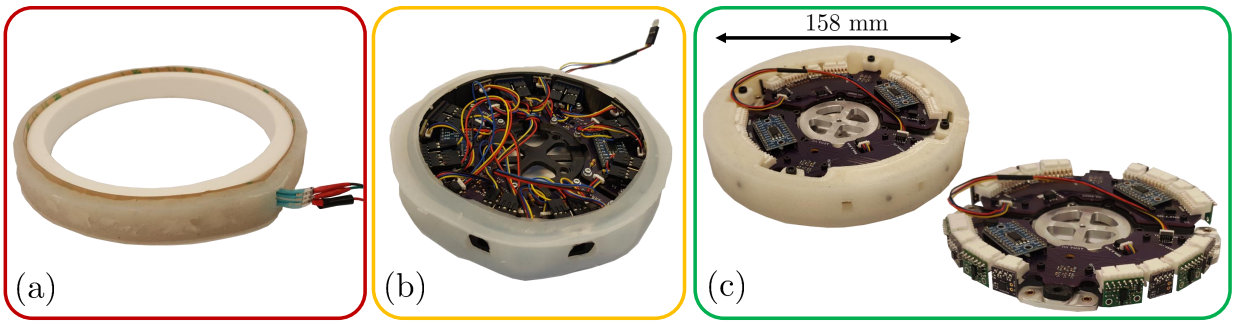

Figure 9: Three design iterations and prototypes of the SDU.

The second design iteration, shown in Fig. 9(b), combined Hall effect and proximity sensing. While functional, this design prevented fast assembly/dissassembly of the sensors due to the wiring required and the fact that sensors were bolted to the plastic outer disk. Furthermore, the silicone layer was mounted by stretching an undersized silicone ring and placing it around the plastic outer cover. With this method, the placement of the magnets within the skin and around

the circumference was neither accurate nor repeatable.

Fig. 9(c) shows our final design that addresses the aforementioned limitations. Board edge connectors are used to mount the individual sensors directly to the PCB. This structure facilitates the assembly and troubleshooting of individual sensors, and significantly reduces the number of cables needed. In addition, the process for fabricating the silicone skin was simplified with new molding fixtures in the final design iteration.

5 Acknowledgments

The authors would like to thank the following people for their assistance in this project:

- Our faculty advisor for feedback on the robot design and funding for the team members.
- Our faculty advisor and an external faculty member collaborator for the initial generation of the design problem and motivating application.
- A government scientific funding agency for their financial support of the project.
- Five undergraduate interns/REU students and a staff engineer for their contributions to the wrist component selection, the printed circuit board design and assembly for microcontroller integration, and the design/assembly of motor control electronics.
- Our university's internal machinist and outside commercial machine shops for fabricating the robot's aluminum parts.

References

[1] M. Vermeulen and M. Wisse, "Intrinsically Safe Robot Arm: Adjustable Static Balancing and Low Power Actuation," *International Journal of Social Robotics*, vol. 2, no. 3, pp. 275–288, sep 2010.

[2] J. A. Collins, H. Busby, and G. Staab, *Mechanical Design of Machine Elements and Machines: A Failure Prevention Perspective*, 2nd ed. Hoboken, NJ: Wiley & Sons, Inc, 2010.

[3] M. Kilic, Y. Yazicioglu, and D. F. Kurtulus, "Synthesis of a torsional spring mechanism with mechanically adjustable stiffness using wrapping cams," *Mechanism and Machine Theory*, vol. 57, pp. 27–39, nov 2012.

[4] K. Xu, Y. Chen, Z. Zhang, S. Zhang, N. Xing, and X. Zhu, "An insertable low-cost continuum tool for shape sensing," in *2017 IEEE International Conference on Robotics and Biomimetics (ROBIO)*. IEEE, Dec. 2017, pp. 2044–2049.

[5] C. G. Frazelle, A. D. Kapadia, and I. D. Walker, "A haptic continuum interface for the teleoperation of extensible continuum manipulators," *IEEE Robotics and Automation Letters*, vol. 5, no. 2, pp. 1875–1882, 2020.

[6] T. Paulino, P. Ribeiro, M. Neto, S. Cardoso, A. Schmitz, J. Santos-Victor, A. Bernardino, and L. Jamone, "Low-cost 3-axis soft tactile sensors for the human-friendly robot vizzy," in *2017 IEEE International Conference on Robotics and Automation (ICRA)*, 2017, pp. 966–971.